Strength of Incompatible Amorphous Polymer Interfaces

Julious L. Willett† and Richard P. Wool*

Department of Materials Science and Engineering, University of Illinois, 1304 West Green Street, Urbana, Illinois 61801

Received January 14, 1993; Revised Manuscript Received June 14, 1993•

ABSTRACT: The mechanical strength of incompatible polymer interfaces welded above T_g was investigated as a function of time, temperature, and composition. Three pairs of polymers were used: polystyrene–poly(methyl methacrylate), poly(styrene-*co*-acrylonitrile)–poly(methyl methacrylate), and poly(styrene-*co*-acrylonitrile)–polycarbonate. For each pair, the weld strength G_{1c}, measured by wedge cleavage, attained a constant value which increased with welding temperature. While the plateau strengths are typically only about 5–10% of bulk G_{1c} values, they are orders of magnitude greater than the work of adhesion calculated using intermolecular forces. For the copolymer–homopolymer pairs, the maximum plateau strength was reached when the Flory–Huggins interaction parameter, χ, was a minimum. These results are in agreement with a model based on Helfand's molecular theories of the structure of incompatible interfaces, coupled with a microscopic deformation mechanism, which predicts that $G_{1c} \sim 1/\chi$. X-ray photoelectron spectroscopy (XPS) and scanning electron microscopy (SEM) analysis of the fracture surfaces revealed dissimilar fracture surfaces for a given pair, with evidence of stick–slip crack growth. XPS revealed residues of one polymer on the other's surface, indicating cohesive fracture occurred to some extent. In each case, the cohesive fracture occurred in the polymer with the lower entanglement density and lower craze stress.

Introduction

When two amorphous polymer surfaces are brought into contact above the glass transition, interdiffusion may occur. Mechanical strength is developed through the formation of an entanglement network across the interface. Polymer–polymer welding is defined as strength development at polymer interfaces through interdiffusion. This process is important in polymer melt processing, coextrusion, lamination, tack of uncured linear elastomers, and polymer blends. Relations between the structure and strength of polymer interfaces and applications are reviewed in ref 1.

Polymer–polymer interfaces can be categorized in four broad groups as follows: symmetric, asymmetric, polymer–nonpolymer, and multicomponent. Symmetric interfaces are formed between polymers having the same chemical composition, such as polystyrene/polystyrene, while asymmetric interfaces are formed by two polymers of unlike composition, polystyrene/poly(methyl methacrylate). Asymmetric interfaces are further subdivided into two classes: compatible and incompatible. Compatible interfaces are relatively few in number compared to the incompatible type since most polymers have a positive enthalpy of mixing and the entropic driving force for mixing is relatively low. The structure and strength of symmetric interfaces have received considerable study, both theoretically[1-5] and experimentally.[6-12] Asymmetric compatible interfaces have also been studied theoretically[13-16] and experimentally.[6,7,17,18] Incompatible asymmetric polymer interfaces have received considerable attention,[19-30] primarily because of their natural abundance and numerous practical applications in blends.

Previous studies of the mechanical properties of polymer interfaces have concentrated on the dynamics of strength development (symmetric and compatible systems) or the influence of the Flory–Huggins interaction parameter χ (compatible and incompatible pairs). Little attention, however, has been paid to the locus of fracture at interfaces, an important aspect in understanding their properties. While chemical analysis of symmetric interface fracture is quite difficult, the chemical differences in asymmetric pairs facilitate the spectroscopic analysis of the fracture surfaces.

The object of this study is 3-fold. First, we determine the fracture energy G_{1c}, of model asymmetric amorphous interfaces as a function of time and temperature using a wedge cleavage fracture mechanics technique. Second, we will analyze the fracture surfaces by XPS and SEM to determine the locus of failure and attempt to ascertain the fracture mechanism. Finally, we relate the strength of the interface to the theoretical structure of the interface using the microscopic analysis. Three families of polymer interfaces are studied: polystyrene/poly(methyl methacrylate) (PS/PMMA) with varying PS molecular weight, poly(styrene-*co*-acrylonitrile)/poly(methyl methacrylate) (PSAN/PMMA) with varying acrylonitrile (AN) content, and poly(styrene-*co*-acrylonitrile)/polycarbonate (PSAN/PC) with varying AN content in the PSAN.

Experimental Section

Sample Preparation. All materials used in this study were glassy amorphous polymers obtained in pellet form, supplied by Dow Chemical Co., Midland, MI. Molding of the pellets into samples suitable for fracture testing was performed as follows. Pellets were dried at least 8 h under vacuum at 90 °C prior to molding, except PC (with a higher glass transition temperature T_g = 150 °C) which was dried at 125 °C. Pellets were transferred to a square mold, 12.5 × 12.5 × 0.32 cm and preheated 20 min at 160 °C under ambient pressure in a Carver press. Molding was done under 800 psi for 20 min at the same temperature. After molding, the press platens were turned off and the pressure was released, while keeping the gap between the top platen and the mold assembly as small as possible. The system was then allowed to cool to room temperature. This procedure produced clear plates which exhibited no birefringence under crossed polars on an optical microscope, indicating the absence of thermal stresses. The only exception to the molding procedure was PC, which was molded at 275 °C due to its crystallization temperature of 240 °C. This material also exhibited no birefringence.

The outer edge (1 cm) of each plate was cut off using a band saw, and the remaining plate was cut into four equal size pieces

* Author to whom correspondence is addressed.
† U.S.D.A. National Center for Agricultural Utilization Research, 1815 N. University Street, Peoria, IL 61604.
• Abstract published in *Advance ACS Abstracts*, September 1, 1993.

0024-9297/93/2226-5336$04.00/0

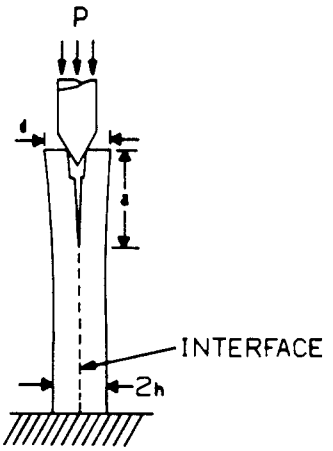

Figure 1. Schematic of the wedge cleavage geometry used to measure G_{1c}.

(5.2 × 5.2 × 0.32 cm). During the machining stage, the aluminum foil against which the materials were molded remained adhered to the outer surfaces and kept them free of contamination and excess scratches. Fracture test specimens were prepared by removing the aluminum foil from two of the 5.2 × 5.2 cm plates (e.g., PS and PMMA), placing them between two brass plates, and inserting the entire assembly into a Carver press at 140 (±1) °C. The top brass plate was then brought into contact with the top platen, but without enough pressure to deform the polymers. After a preheat period of 120 s, the lower platen was raised until slight pressure was exerted on the polymer surfaces, which promoted good contact (wetting) between the surfaces. After a wetting period of 120–180 s depending on the materials, the assembly was removed and placed under metal weights at room temperature to cool rapidly. Any pair of plates which decreased in thickness more than 5% was discarded. This guideline was adopted to minimize pressure effects on wetting and sample distortion effects on fracture. A sample assembly with a thermocouple inserted in the interface indicated the temperature reached 138–140 °C after about 140 s and remained fairly constant afterward. With practice, reproducible wetting results were obtained.

The wetted sample plate was then cut into strips 1 cm in width, a single 5.2 × 5.2 cm sandwich yielding 4 or 5 samples. This procedure allowed production of several samples with identical thermal histories. Into one end of each strip, a crack was initiated at the interface to a length of 8–10 mm by lightly tapping a razor blade into the interface. A notch was then cut into this end with a jeweler's saw to a depth of about 3 mm, and all rough edges were sanded down.

For cases where a material was in short supply or quite expensive as in the case of monodisperse PS, a slight variation of the above procedure was used. Instead of a 3.2-mm-thick plate, a 2.2-mm-thick one was molded of a suitable backing material, e.g., polydisperse PS, and a 1-mm-thick molded plate of the less plentiful material was then glued onto it with Devcon 5-min epoxy. This technique has been used previously in symmetric welding studies and was found to perform in a suitable manner.[31] Machining and wetting was done the same as described above for these samples.

To avoid moisture sorption problems, all materials were kept in a vacuum desiccator when not in use.

Welding and Fracture Energy Measurement. A geometry ideally suited to interface welding studies is wedge cleavage, illustrated in Figure 1. Similar to the double-cantilever beam, the technique involves driving a wedge into the top of a sample at 23 °C. As the wedge is driven downward, the top halves of the sample are forced apart. At a critical separation, crack growth begins and advances along the middle of the sample (in the ideal case). If the motion of the wedge is halted and the system allowed to equilibrate, the crack will advance until the stress concentration at its tip is no longer sufficient to cause further crack growth. Under this constant displacement condition, the following relation may be used to determine G_{1c}[32]

$$G_{1c} = (3/16)[(d-2h)^2Eh^3/a^4]F(h/a)\,Q(h) \quad (1)$$

where d is the separation across the outside surfaces at the top of the sample, $2h$ is the sample thickness, E is the elastic modulus, and a is the crack length. The function

$$F(h/a) = 1/[1 + 0.64(h/a)]^4 \quad (2)$$

accounts for the system compliance; $Q(h)$ accounts for the groove contribution to the compliance and is close to 1. The utility of this technique in interface welding studies has been previously demonstrated.[8,9,33,34]

The welding experiments were performed in the following manner. After measuring the initial wetting strength of samples prepared as described above, three samples were placed in the slots of a metal template preheated in a vacuum oven to the desired welding temperature. The template and samples were covered with a brass plate, and a metal bar was also maintained at the welding temperature. The entire assembly, weighing approximately 1 kg, was placed back in the vacuum oven, which was then evacuated. After evacuation, N_2 was introduced into the oven until a pressure of 0.5 atm was reached. After a specified period of time, on the order of 1500 s, the template was removed from the oven and quenched between large metal masses at room temperature. Within 2–3 min, the assembly was cool enough to remove the samples. After equilibration to room temperature, cracks were reinitiated in the samples and G_{1c} measured.

The purpose of the template was 2-fold. First, it provided a large thermal mass which allowed rapid heat-up of the samples to the desired temperature; the weight ratio of the metal to the samples was roughly 100:1. The time to achieve the desired welding temperature was typically 2–3 min, measured by placing a dummy sample with a thermocouple probe in its interface into the template. Second, the slots in the template maintained sample integrity. Samples welding between brass plates with no lateral constraint flattened substantially due to flow at the elevated welding temperatures. By carefully machining the samples to fit snugly in the slots in the template, deformation during welding was minimized.

Measurement of G_{1c} proceeded as follows. A sample was mounted in the lower grip of an MTS model 820 servohydraulic testing machine, and the wedge in the upper grip was aligned with the notch on top of the specimen. The lower grip then moved up at a rate of 0.25 mm/min. The sample was illuminated from the rear to make the crack more visible, and the crack was observed with a traveling microscope during the loading process. Once the crack began to grow into previously nonfractured material, the actuator movement was halted and the crack allowed to come to rest (normally after 3–5 min). Typically, crack growth was slow, about 2–3 mm/min. At this point, the displacement d (of eq 1) was measured to within 0.01 mm with a screw micrometer, the actuator was returned to its initial position, and the sample was removed. The crack length a was measured to within 0.01 mm with Vernier calipers. This procedure was repeated 3–5 times for each sample. Values of G_{1c} were evaluated using measured d and a results, specimen parameters, and modulus values determined from three-point bend tests. For a typical set of data at a constant welding time involving 16–25 data points, the standard deviation was about 10–15% of the mean. Repetition of the welding and measurement process allowed the construction of G_{1c} versus time curves from one set of samples.

X-Ray Photoelectron Spectroscopy. XPS spectra were recorded on a Philips Electronic Model 548 spectrometer using a Mg X-ray (nonmonochromatic) source and a cylindrical mirror analyzer. The incident beam spot size was approximately 7 mm², and the spectra represent the average composition of an area that size. Chamber pressures were on the order of 10^{-9} Torr during spectra measurements.

Atomic ratios of oxygen to carbon (O/C) and nitrogen to carbon (N/C) were determined by measuring the peak areas A_i, for each element i = O, C, N, and converting the area ratios to atomic ratios using atomic sensitivity factors S_i. S_i is a measure of the cross section of each element in the X-ray electron ejection process, relative to fluorine ($S_F = 1$). Atomic ratios were obtained

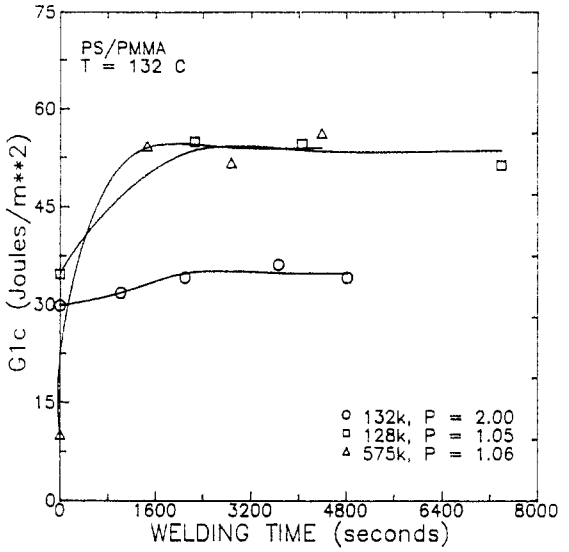

Figure 2. Effect of PS molecular weight on the weld strength of PS/PMMA interfaces. T_w is 132 °C.

Table I. PS and PMMA Properties

	M_n	M_w	modulus (psi)	T_g (°C)
PS	132 000	302 000	390 000	100
PS	128 000	134 000	390 000	105
PS	575 000	609 500	390 000	105
PMMA	62 000	120 000	390 000	108

using the relations

$$\frac{N}{C} = \frac{(A_N/S_N)}{(A_C/S_C)} \tag{3}$$

$$\frac{O}{C} = \frac{(A_O/S_O)}{(A_C/S_C)} \tag{4}$$

By comparing atomic ratios of the pure (as molded) polymer surfaces with those of the fracture surfaces, we can sensitively determine the composition of the surface. Since the XPS electron escape depths are low, the composition analysis is conveniently confined to a depth of a few nanometers, which is a typical equilibrium depth of incompatible interfaces.

Microscopic Analysis. Approximately a 1-cm² section of one side of a fractured wedge cleavage sample was glued to an aluminum base. The fracture surface was marked to indicate the direction of crack propagation. The sides of the sample were coated with a conductive adhesive, DAG 154, to minimize charging in the SEM. The adhesive dried for 24 h, and the surfaces were sputter coated with gold for 2 min, resulting in a gold coating of approximately 150–200-Å thickness. Optical microscopic examination (Aus-Jena microscope equipped with polarizers and a birefringence analyzer) of the surfaces before and afte the coating process indicated no thermal artifacts were introduced by this preparation method. A JEOL Model JSM-35C was used for the SEM analysis.

Weld Strength Results

PS/PMMA Strength. The fracture energy of PS/PMMA interfaces welded at 132 °C is shown in Figure 2 as a function of weld time for three PS molecular weight distributions listed in Table I. The results are characteristic of all the incompatible pairs studied. The strengths at zero welding time are due to the initial wetting. With time, the strength increases to a plateau G_{1c} value (ca. 50 J/m²) and remains constant thereafter. The equilibrium strength is less than about a tenth of the fracture energy (500–1000 J/m²) of either bulk polymer but much greater than the work of adhesion, discussed below.

No difference is seen between the plateau strength of the two monodisperse molecular weight (128K and 575K) PS samples. However, the polydisperse (132K) PS sample shows a lower strength which may be due to molecular weight segregation effects at the interface. Related studies by Foster and Wool[34] using the same polydisperse PS/PMMA materials found $G_{1c} = 42.5 \pm 4.5$ J/m², which is very close to this study. The time to achieve the plateau strength is about 1600 s for all molecular weights. While these experiments, unlike our symmetric interface studies,[8,9] were not designed to analyze the dynamics of strength development, a few comments are appropriate. The dynamics of strength development at interfaces is controlled by two convoluted time-dependent functions, wetting and diffusion.[8] Unless care is taken to minimize the wetting function, the contribution from the diffusion function becomes masked by the convolution process.

For symmetric PS/PS interfaces, Whitlow and Wool[35] have shown from SIMS experiments that the interface thickness d increases with time t as

$$d(t) = 2R_g[t/T_r]^{1/4} \tag{5}$$

where $T_r \sim M^3$ is the reptation time and R_g is the radius of gyration. The exponent of $^1/_4$ is due to the correlated motion of the chains at $t < T_r$. When $t > T_r$, the correlations are lost and the usual Fickian diffusion result is obtained with $d(t) \sim t^{1/2}$.

For incompatible interfaces, the interface reaches an equilibrium thickness d_∞, which, according to Helfand,[19,20] is a balance between the adverse enthalpy of mixing and a favorable entropy gain of the molecules on the surface layer, such that

$$d_\infty = 2b/(6\chi)^{1/2} \tag{6}$$

where b is the statistical segment length ($b = 6.5$ Å for PS and PMMA) and χ is the Flory–Huggins interaction parameter. If we assume that the interface dynamics is largely dominated by reptation, then the interface thickness d_∞ develops at a time t_∞ derived from eq 5 as

$$t_\infty = [d_\infty/2R_g]^4 T_r \tag{7}$$

Since $R_g \sim M^{1/2}$ and $d_\infty \sim M^0/\chi^{1/2}$, the molecular weight dependence of the reptation controlled equilibration time is obtained as $t_\infty \sim M$. If this relation were applicable, we would expect a stronger molecular weight dependence of the time to achieve the plateau strength in Figure 2. Also, substituting typical values for $d_\infty \approx 50$ Å, $R_g \approx 100$ Å, and $T_r \approx 3000$ s for $M = 132\,000$ at 125 °C, we obtain $t_\infty \approx 10$ s, which is much shorter than the observed welding time of about 2000 s.

For welding of symmetric amorphous interfaces (reviewed in ref 1), we have argued[8,9,36] that $G_{1c} \sim d^2$, and if we assume for the asymmetric interface that $G_{1c} \sim d_\infty^2$, then we have[9,34]

$$G_{1c} = 1/4G_0(d_\infty/R_g)^2 \tag{8}$$

where G_0 is the strength of a symmetric interface of thickness $2R_g$. This relation assumes that the molecular weight is in the range $2M_e < M < 16M_e$. For the monodisperse molecular weight PS with $M = 128\,000$ shown in Figure 2, $R \approx 100$ Å, $G_{1c} \approx 50$ J/m², and $G_0 \approx 500$ J/m² for the symmetric PS/PS interface. From eq 8, we estimate that $d_\infty \approx 60$ Å. Equation 8 assumes that the deformation zone at the crack tip of an A/B interface forms symmetrically about the crack plane, as with the symmetric A/A interface. We will see later from the microscopic analysis of the fracture surfaces that this assumption is often not valid.

When $G_{1c} \sim d_\infty^2$, then we expect the fracture energy to depend on the Flory–Huggins parameter as

$$G_{1c} \sim 1/\chi \tag{9}$$

The χ parameter is usually a function of temperature (K) as

$$\chi(T) = A/T + B \tag{10}$$

where A and B are constants. Russell et al.[37] determined $\chi(T)$ for PS/PMMA as

$$\chi = 3.902/T + 0.0284 \tag{11}$$

Due to the small A factor in eq 10, χ for this interface has very little temperature dependence, which is consistent with fracture strength observations. Using Helfand's theory (eq 6) with $\chi = 0.038$, this gives $d_\infty \approx 27$ Å at 132 °C. Neutron reflection experiments on PS/PMMA interfaces by Russell et al.[37] give $d_\infty \approx 50 \pm 10$ Å which is larger than the theoretical value but of comparable order of magnitude.

A comparison of the magnitude of the plateau G_{1c} values of Figure 2 with theoretical predictions of the work of adhesion, W_{12}, provides further support for the interpenetration hypothesis. The thermodynamic work of adhesion W_{12} is given as[37]

$$W_{12} = \Gamma_1 + \Gamma_2 - \Gamma_{12} \tag{12}$$

where Γ_1 and Γ_2 are the surface tensions of phases 1 and 2, and Γ_{12} is the interfacial tension. Substituting appropriate values for PS and PMMA into eq 12, W_{12} is calculated to be 0.08 J/m² at 25 °C. The thermodynamic work of adhesion is about 500 times smaller than the measured G_{1c} values. Analyses based on van der Waals dispersion forces between two infinite plates[38] and acid–base interactions[39,40] gave similar results.[33]

The case of shear at the interface between two incompatible polymers was examined by Brochard, de Gennes, and Troian.[41] If A and B are not entangled ($d_\infty < N_e^{1/2}$), they expect a weak Rouse friction with viscosity η_R, which is size dependent, as

$$\eta_R = \eta_1(d_\infty/b)^2 \tag{13}$$

Here b is the length of a statistical segment and η_1 is the viscosity of monomers. For very weak interfaces, at $d_\infty \approx b$, $\eta_R \to \eta_1$, and when $d_\infty \approx N_e^{1/2}b$, $\eta_R \to \eta_1 N_e$, where N_e is the number of monomers in the entanglement molecular weight. If V is the sliding velocity, then the stress σ can be represented by

$$\sigma = \eta_R V/d_\infty \tag{14}$$

where V/d_∞ is the shear rate. Using eq 13, this predicts that $\sigma \sim d_\infty$ and the energy to create unit fracture surface area in shear is $G_{III} \sim \sigma^2$ which gives $G_{III} \sim d_\infty^2$. This is similar to the mode I fracture case (eq 8) which we presented above.

PSAN/PMMA Strength. Another method of changing the interaction parameter other than temperature is chemically, using a copolymer as one of the components of the interface. This approach provides another route to investigate the role played by the interaction parameter in determining the weld strength of incompatible polymer interfaces. The materials chosen for this study were the same PMMA used in the PS study and three PSANs of various AN content. Their characteristics are given in Table II.

The interaction parameter χ for a copolymer–homopolymer pair with random mixing can be expressed as

Table II. PSAN Properties

% AN	M_n	modulus (psi)	T_g (°C)
5.7	136 000	397 000	106
23	75 000	439 000	108
37	68 000	469 000	109

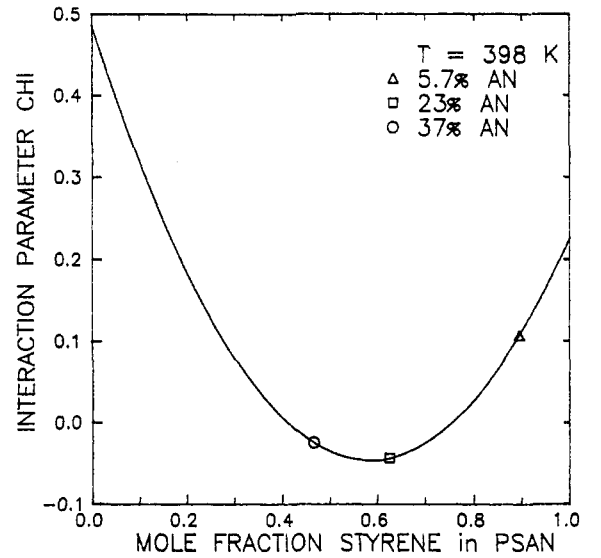

Figure 3. Interaction parameter χ for PSAN/PMMA as a function of the mole fraction of styrene in the PSAN. $T = 125$ °C.

$$\chi = \beta\chi_{13} + (1-\beta)\chi_{23} - \beta(1-\beta)\chi_{12} \tag{15}$$

where χ_{ij} is the interaction parameter between monomers i and j, 1 and 2 are the comonomers, 3 is the homopolymer, and β is the mole fraction of monomer 1 in the copolymer. Equation 15 therefore calculates χ based on random mixing of the homopolymer with a random copolymer.

The quadratic relationship between χ and β has two important consequences. First, χ has a minimum at β^*

$$\beta^* = 0.5(\chi_{12} + \chi_{23} - \chi_{13})/\chi_{12} \tag{16}$$

which implies that this composition will have the greatest welding strength. Second, if $\chi_{12} > [\chi_{23} + \chi_{13}]^2$, this minimum is negative, and a range of compositions exists where the two materials are compatible. In this composition range, welding strength will be controlled by center-of-mass interdiffusion back and forth across the interface, leading to fracture strengths on the order of bulk strengths.

Using χ values for PMMA, PAN, and PS of Kressler et al.[45] one has the following relation:

$$\chi = T^{-1}(624\beta^2 - 727\beta + 193) \tag{17}$$

where β is the mole fraction of styrene in the copolymer. The numerical coefficients include all the terms indicated in eq 15 for the interaction between each pair of monomers (S/MMA, S/AN, AN/MMA). A plot of eq 17 is shown in Figure 3. Differentiating eq 17 with respect to β, one finds the minimum value of χ at $\beta^* = 0.58$. This value corresponds to a weight percent AN of 27%. The minimum value of χ is −0.05 at 125 °C, which predicts compatibility. In fact, the range of composition which gives compatibility is $0.41 < \beta < 0.75$, which corresponds to AN contents of 15–42%. Therefore, the copolymers with 23.4% AN and 37% AN are predicted to be compatible with PMMA, while the 5.7% AN copolymer should be incompatible, but have a higher weld strength than pure PS with PMMA.

The results of PSAN/PMMA interfaces welded at 140 °C are shown in Figure 4. The same general features are

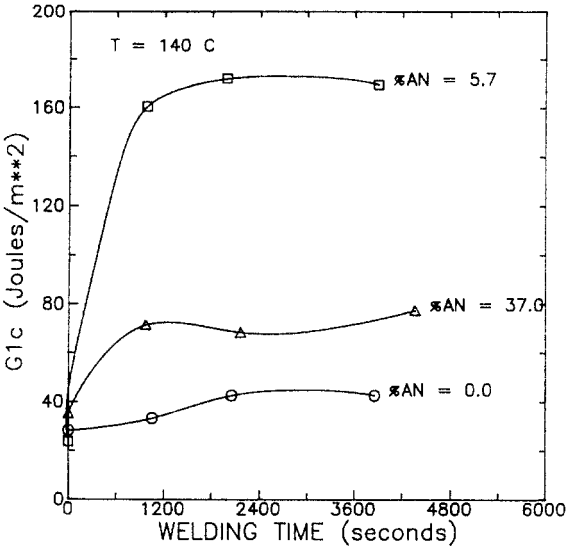

Figure 4. Weld strength as a function of time for three PSAN/PMMA interfaces. T_w = 140 °C.

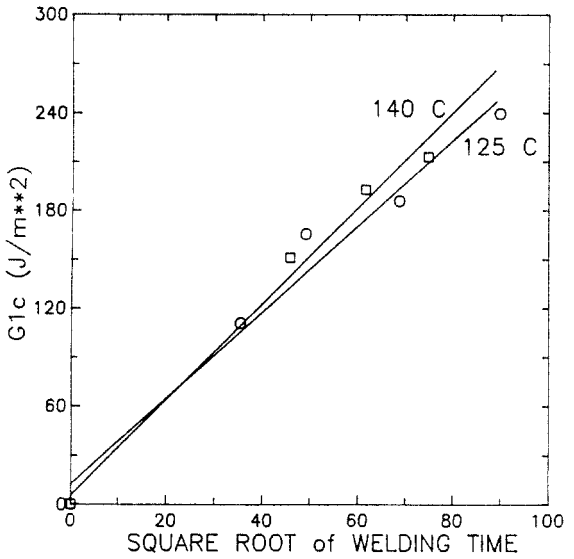

Figure 5. Weld strength versus the square root of time for the compatible PSAN/PMMA pair.

seen as for PS/PMMA welding. While the 5.7% AN/PMMA pair behaves as expected relative to PS, the 37.0% AN copolymer's behavior indicates it is incompatible with PMMA, in contradiction with eq 17. One explanation for this departure from theory is the random mixing assumption used in deriving this equation. This assumption neglects any configurational or comonomer sequence effects on χ. Such effects have been studied and shown to affect the validity of eq 17.[46-48] Since the 37% AN copolymer has a nearly 1:1 molar ratio of styrene to acrylonitrile monomers (see Figure 3), these effects are probably important and lead to an incorrect calculation of χ.

The 23.4% AN copolymer, on the other hand, exhibited completely different welding behavior with PMMA, as shown in Figure 5. Not only are the levels of strength much greater at both temperatures but no plateau seems apparent even after 6000 s. These results are consistent with the prediction of compatibility for this pair. Using the minor chain model for polymer welding[4,8] and assuming a disentanglement dominated fracture mechanism, a $t^{1/2}$ time dependence is predicted for G_{1c}. A plot of G_{1c} against the square root of welding time exhibits reasonable linearity. Similar behavior has been observed by Kausch et al. in crack healing experiments with PMMA and a 25% AN[6,7] copolymer, which also forms a comparible pair.

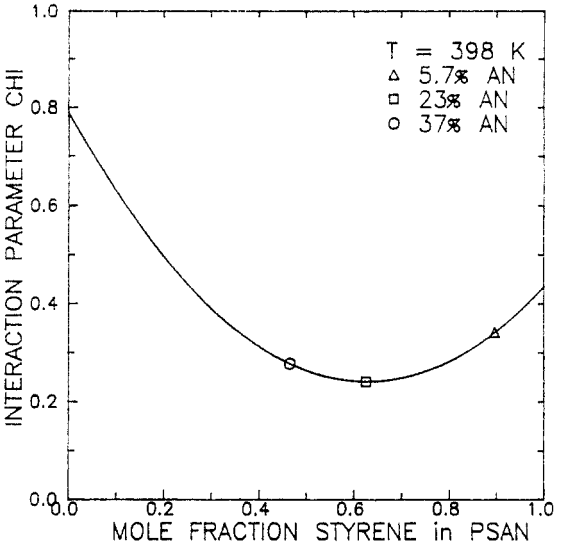

Figure 6. Interaction parameter χ for PC/PSAN interfaces versus the mole fraction of styrene in the PSAN. T = 125 °C.

The incompatibility–compatibility transition with AN content is confirmed by the optical appearance of cast films of PSAN/PMMA mixtues. Solutions of 50/50 (w/w) were prepared in methylene chloride at a concentration of 1.0 g/dL. Films were cast after 24 h of dissolution time. The 23.4% AN copolymer/PMMA blend formed a clear film with no visible phase separation after annealing at 125 and 140 °C. The other three films (0.0%, 5.7%, and 37.0% AN) exhibited phase separation in the form of spherical droplets; annealing did not visibly alter their appearance. These results are in agreement with other studies of the compatibility of PSAN/PMMA blends.[49,50]

PC/PSAN Strength. The third pair considered in these welding experiments was PC/PSAN. This pair is of some practical importance as PC/ABS blends have been the subject of considerable interest in recent years. The same three PSAN copolymers used in the previous work were used in this study; their characteristics are given in Table II. The molecular weight of the PC was $M_n \approx 28\,000$, its T_g was 150 °C, and its modulus was 280 kpsi. Of particular interest in this system is the large discrepancy between the glass transition temperatures of the two types of polymers. This difference allows welding to be studied in two regions: between the T_gs of the two polymers (a 40 °C difference) and above T_g of the PC. Only welding at or below T_g of the PC will be discussed here.

As in the PSAN/PMMA case, the AN content allows one to change χ without changing the temperature, accordingly[33]

$$\chi = T^{-1}(556\beta^2 - 697\beta + 314) \qquad (18)$$

with β again being the styrene mole fraction in the PSAN. A plot of this function is given in Figure 6. In this case, χ is nowhere negative, so one would expect all three PSAN copolymers to behave in the incompatible fashion seen in the previous systems. The minimum value of χ occurs at $\beta^* = 0.63$, which corresponds to a copolymer of 23% AN and should exhibit the highest weld strength with PC.

G_{1c} curves for PSAN/PC interfaces welded at 125 °C are shown in Figure 7. The familiar shape for incompatible polymer interfaces is seen, with strengths of the same order of magnitude as the other two systems. These results suggest that a certain amount of interdiffusion is taking place, even though the PC is still more than 20 °C below

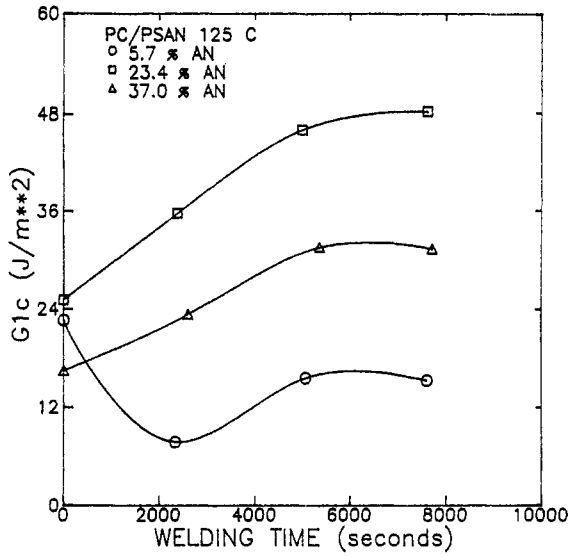

Figure 7. Weld strength as a function of time for PC/PSAN interfaces. T_w = 125 °C.

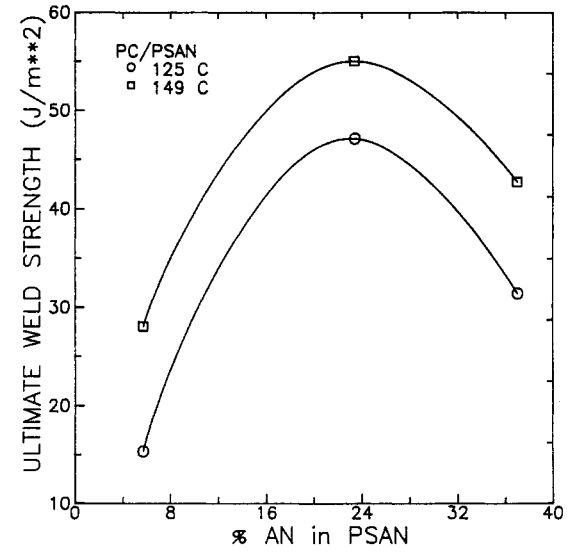

Figure 8. Effect of copolymer composition on the plateau strength of PC/PSAN interfaces.

its T_g. This mixing may be a result of a plasticizing action of the more fluid PSAN (T_g(PSAN) < T_g(PC)) on the PC during welding.

The composition of the PSAN has a marked effect on the ultimate weld strength as evidenced by the fact that the 23.0% AN copolymer weld strength is 3 times larger than that of the 5.7% AN. This composition dependence clearly indicates the role that the interaction parameter plays in determining the weld strength of polymer interfaces. Similar results were obtained near T_g at 149 °C.

The temperature and composition results are condensed in Figure 8. At each temperature, the 23.0% AN copolymer exhibits the maximum ultimate strength of the interfaces studied. This composition is also the one which eq 17 predicts will have the highest strength. In addition, since eq 17 gives χ(37.0% AN) < χ(5.7% AN), one would expect the 37.0% AN copolymer to exhibit the higher strength of the two; this is indeed observed. Although the calculation of χ involves several assumptions, the correlation between the calculated values and the plateau strength indicates the importance of χ in determining the ultimate strength of incompatible polymer interfaces.

The effect of composition dependence for this system is similar to the results of Keitz and co-workers,[51] who observed a maximum in the fracture strength of PC/PSAN interfaces, measured by lap shear, at an AN composition of about 24%. Their welding conditions were given as 8 min at 190 °C, under slight pressure. Thus, it is observed that the optimum PSAN composition is reflected for welding both above and below T_g of the PC.

Keitz et al.[51] and Mendelson[52] have shown that when melt blended at temperatures in the neighborhood of 220 °C, PC and PSANs of various composition are in fact partially miscible. By measuring the changes in T_g of each material when blended relative to pure phase T_gs, they were able to calculate the composition of each phase. For several different blend ratios of PC and PSAN, the peak weight fraction of PC in the PSAN phase always occurred at the PSAN composition which gave the highest lap shear strength; the weight fraction of PSAN in PC was somewhat insensitive to the AN content. Typical maximum values for PC in PSAN were 15–20%, while only 10% or less by weight PSAN was measured in the PC phase.

XPS Analysis of Fracture Surfaces. While the experimental results of the previous section are in good agreement with the welding picture of incompatible polymer interfaces, a complete understanding of the mechanical properties of these interfaces requires knowledge of the actual interface breakdown process and subsequent crack growth. Analysis of the fracture surface chemistries will tell whether fracture is adhesive (at the interface) or cohesive (in one or the other bulk), or a combination of the two modes.

The technique used to characterize the chemical nature of the fracture surfaces was X-ray photoelectron spectroscopy (XPS). Fracture surfaces are irradiated with X-rays, usually from either a Mg or Al source. The X-rays eject electrons from the chemical groups, and their characteristic kinetic energies give the chemical composition of the surface. Since the escape depth of electrons is only 20–30 Å for most organic materials,[53] XPS provides a powerful surface analysis technique. This technique is particularly useful to this study due to the fact that the PSAN copolymers all contain nitrogen, which is absent in the materials to which they are welded. Therefore, the presence (or absence) of nitrogen on the fracture surfaces of the other polymers will provide crucial insight into the fracture process. The peak positions of the three elements of interest are the C_{1s} peak near 285 eV, the O_{1s} peak near 540 eV in the PMMA spectra, and the N_{1s} peak near 400 eV in the PSAN spectra. We used the areas of the 1s peaks to determine atomic ratios.

XPS Analysis of PS/PMMA Fracture Surfaces. Spectra from 250 to 550 eV for PMMA fracture surfaces welded to PS at 125 and 140 °C are shown in Figure 9. The C_{1s} peak is near 285 eV, and the O_{1s} peak is near 540 eV. The O_{1s} peaks of the fracture surfaces at both temperatures are clearly reduced relative to C_{1s} peaks, indicating an increase in the carbon content. O/C ratios for these two spectra are 0.26 and 0.28, respectively. In contrast, the O/C ratio of as-molded PMMA, shown in Figure 9a, is 0.38, in good agreement with the theoretical value of 0.40 (2 oxygen atoms and 5 carbon atoms per monomer).

O/C ratios measured on the corresponding PS fracture surfaces are on the order of 0.01 or less. The PS fracture surfaces are indistinguishable from as-molded PS surfaces. Foster and Wool obtained similar results in a related study of PS/PMMA interfaces.[34] These results show that crack growth at PS/PMMA interfaces is both cohesive and adhesive in nature. Cohesive fracture occurs only in the PS side to the extent that XPS analysis can detect. If the fracture were completely adhesive, we would expect an

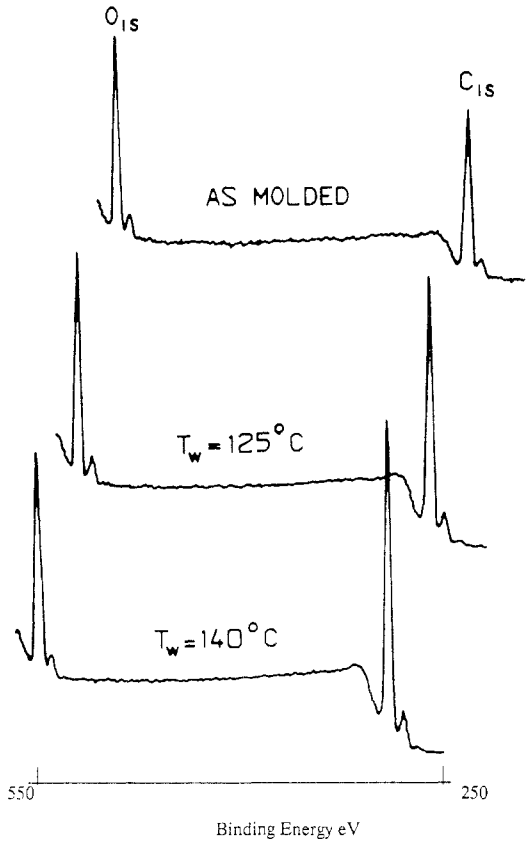

Figure 9. XPS spectra of PMMA fracture surfaces welded to PS: (a) as molded; (b) T_w = 125 °C; (c) T_w = 140 °C. Range is 250–550 eV.

O/C ratio of about 0.38 for the PMMA side; if the fracture were completely cohesive (in PS), we would expect O/C $\approx$ 0. Thus, the approximate relative contribution of each failure mode, as estimated by the ratio 0.38/0.28 $\approx$ 0.74 suggests that the fracture process is more adhesive than cohesive (about 3:1) for a PS/PMMA interface.

XPS Analysis of PSAN/PMMA Fracture Surfaces. XPS spectra of PMMA fracture surfaces welded to PSAN with different AN content at 125 °C are shown in Figure 10. N_{1s} peaks near 400 eV are apparent on each PMMA fracture surface. The O_{1s} peak on the PMMA welded to PSAN1 (% AN = 5.7) is greatly reduced, and virtually no O_{1s} signal is measured on the surface welded to PSAN2 (% AN = 23.4). The N/C values for these spectra are 0.013 and 0.072, respectively. The O/C values are 0.065 and 0.009, substantially less than the as-molded PMMA value of 0.38. By comparison, the N/C values for as-molded PSAN1 and PSAN2 are 0.015 and 0.068, while the theoretical values are 0.016 and 0.061, respectively. These results show that fracture of welded PSAN1/PMMA and PSAN2/PMMA interfaces is almost purely cohesive. With PSAN3 (% AN = 37.0) at 125 °C, nitrogen is detected Figure 10, but to a much smaller extent than with PSAN1 and PSAN2. The O/C value is 0.36, and the N/C value is 0.013. The as-molded N/C value for PSAN3 is 0.101; the theoretical value is 0.106. When the welding temperature was increased to 140 °C, similar results were obtained (Table III). PSAN1 and PSAN2 exhibit purely cohesive failure, while at both temperatures PSAN3 exhibits a combination of cohesive and adhesive failure.

Analysis of the PSAN fracture surfaces indicates no measurable cohesive fracture occurred in the PMMA. In all three cases, the N/C values measured on PSAN fracture surfaces were equal to as-molded values, within experimental error. O/C values of 0.01–0.03 were measured on

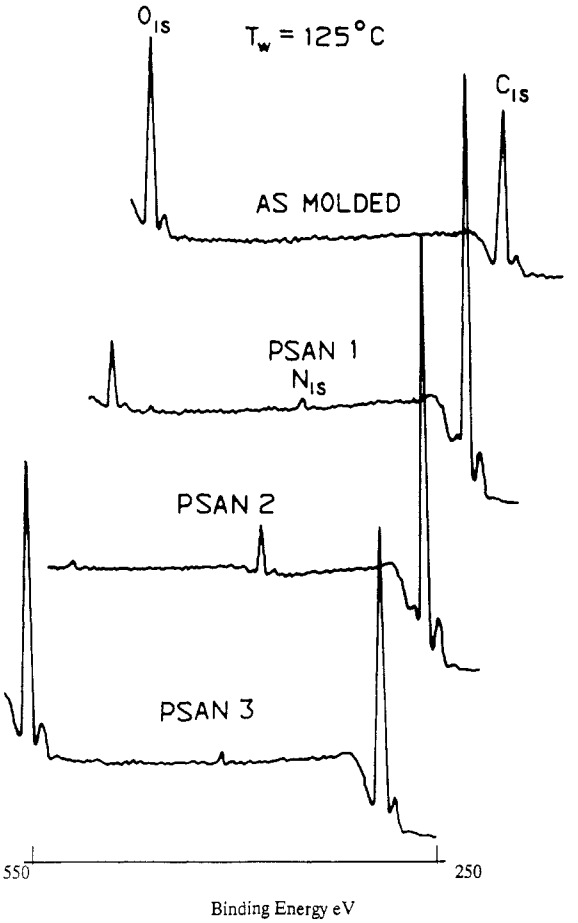

Figure 10. XPS spectra of PMMA fracture surfaces molded to PSAN copolymers: (a) as molded; (b) 5.7% AN; (c) 23% AN; (d) 37% AN. T_w = 125 °C. Range is 250–550 eV.

Table III. N/C Ratios from PMMA Fracture Surfaces

		PMMA		PSAN	
	% AN	N/C	O/C	N/C	O/C
125 °C	0		0.26		0.009
	5.7	0.013	0.065	0.017	0.005
	23	0.072	0.009	0.066	0.011
	37	0.013	0.361	0.101	0.045
140 °C	0		0.279		0.010
	5.7	0.012	0.007	0.014	0.006
	23	0.069	0.010	0.070	0.007
	37	0.021	0.333	0.100	0.032
theoretical N/C values					
	5.7	0.016			
	23	0.061			
	37	0.106			

as-molded PSAN surfaces as well as PSAN fracture surfaces. This oxygen content may be due to oxidation of acrylonitrile groups during molding.

The presence of cohesive fracture at all the interfaces studied, particularly with PSAN1 and PSAN2, indicates the "interface" fracture process can be dominated by deformation processes occurring in the bulk phases. Therefore, any comparison between models of interface strength and measurements must account for the role of cohesive fracture. Clearly, interfaces between incompatible polymers can attain sufficient strength to shift the locus of fracture to one of the bulk materials.

XPS Analysis of PC/PSAN Fracture Surfaces. Figure 11 illustrates the XPS spectra obtained from PC fracture surfaces welded to PSAN at 125 °C, which is below the T_g of PC. As in the PMMA case, an N_{1s} signal is detected for all three PSANs. A decrease in the O/C ratio is also evident relative to the value for as-molded PC. These

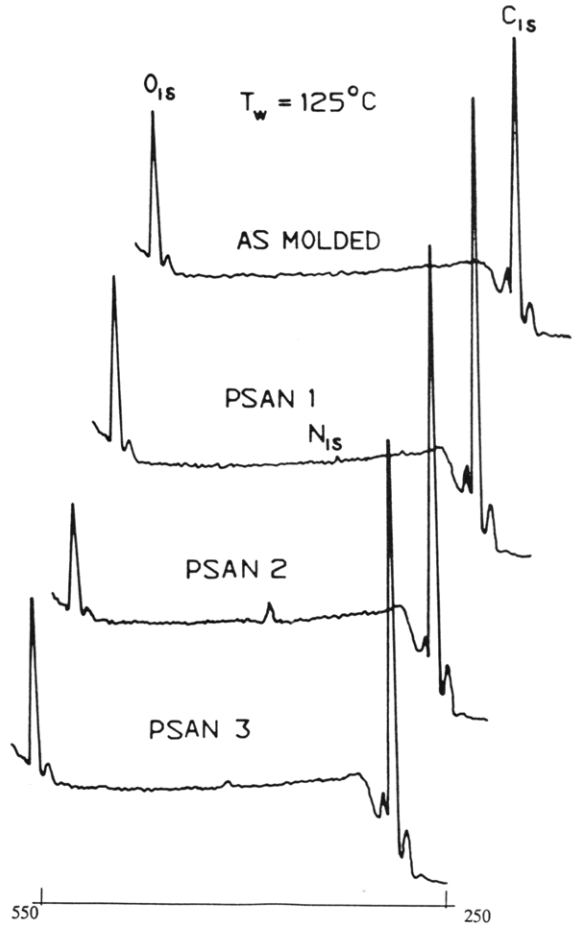

Figure 11. XSP spectra of PS fracture surfaces welded to PSAN: (a) as molded; (b) 5.7% AN; (c) 23% AN; (d) 37% AN. T_w = 125 °C. Range is 250–550 eV.

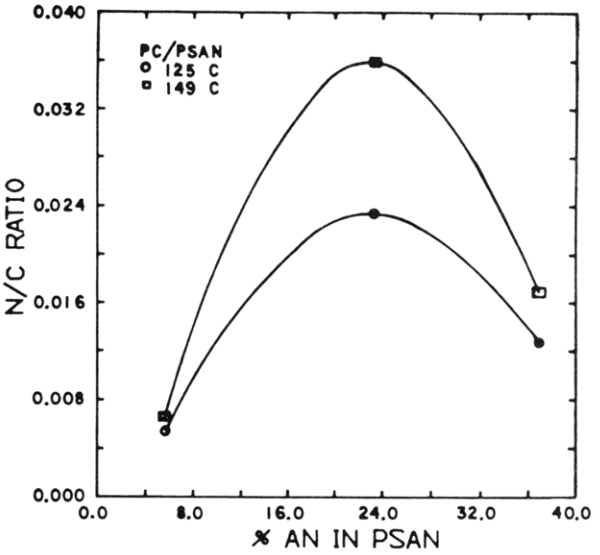

Figure 12. Nitrogen/carbon ratios measured on PC fracture surfaces versus % AN.

results indicate cohesive fracture occurred even though the welding temperature was lower than T_g of the PC. Similar results were obtained for PC fracture surfaces welded at 149 °C, which is at the T_g of PC.

Figure 12 shows the N/C ratios plotted against the acrylonitrile content of the PSAN copolymers. At both welding temperatures, the maximum N/C ratio corresponds to PSAN2 (23.4% AN), followed by PSAN3 and

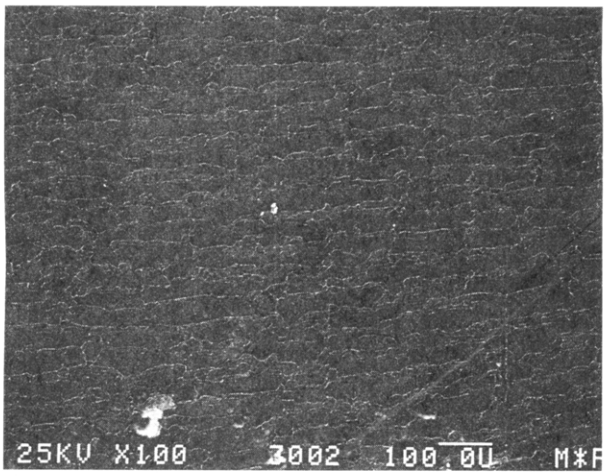

a

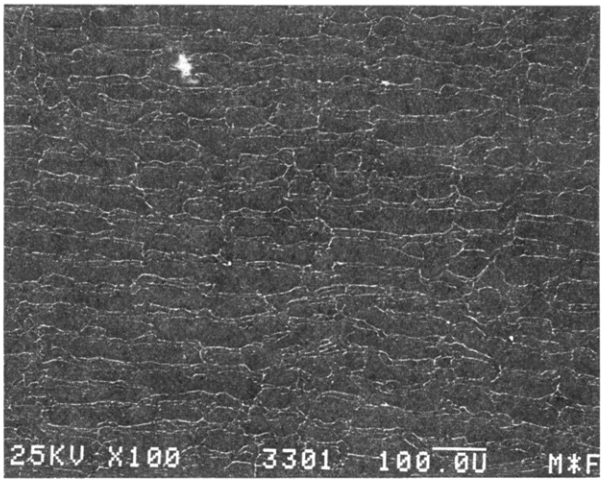

b

Figure 13. SEM micrographs of PS fracture surfaces welded to PMMA: (a) T_w = 125 °C; (b) T_w = 140 °C. Magnification 100×.

PSAN1. The measured fracture energies (Figure 8) follow the same trend, with PSAN2 having the largest interface strength with PC. In addition, the correlation between the N/C ratios and weld strength, and the acrylonitrile content, agrees with interaction parameter calculations which exhibits a broad minimum near 25% AN.

SEM Analysis of Fracture Surfaces. SEM Analysis of PS/PMMA. Representative SEM images of a PS fracture surface welded to PMMA at 125 and 140 °C are shown in Figure 13. The most striking feature of these and other PS surfaces is their similarity, despite their different welding conditions and molecular weights. All surfaces shown are characterized by a series of lines, hundreds of microns in length with a well-defined spacing of roughly 50 μm, which are perpendicular to the direction of crack growth.

At higher magnification, these lines are seen to be composed of several ridges of highly deformed material, as shown in Figure 14. These ridges exhibited birefringence when viewed through crossed polars. Given that the XPS analysis showed PS fracture surfaces are pure PS, it is clear these ridges are highly deformed PS and not PMMA residues. These features are indicative of discontinuous "stick–slip" crack growth. This type of un-

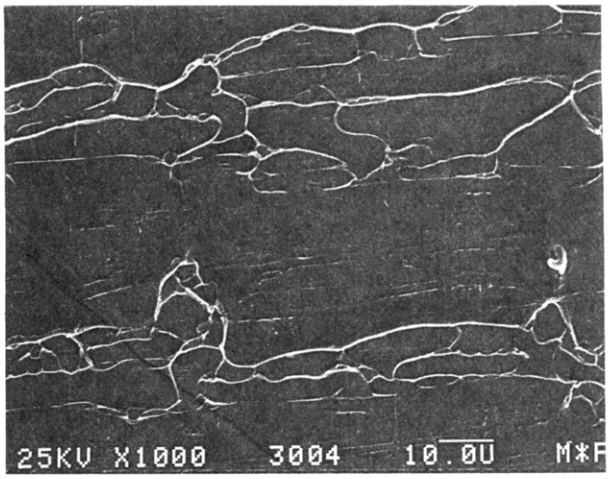

a

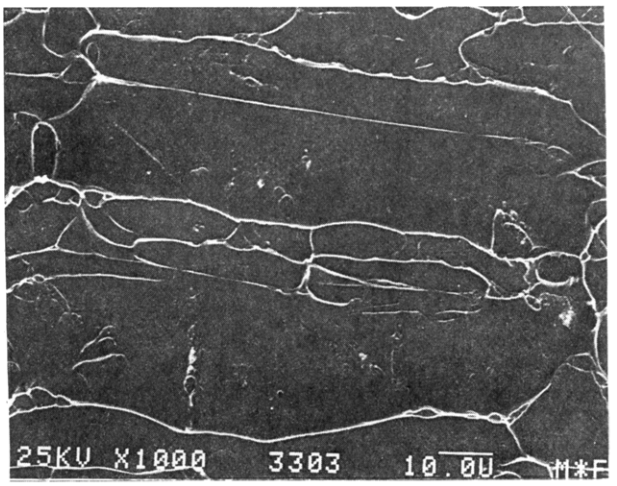

b

Figure 14. SEM micrographs of PS fracture surfaces to PMMA: (a) $T_w = 125$ °C; (b) $T_w = 140$ °C. Magnification 1000×.

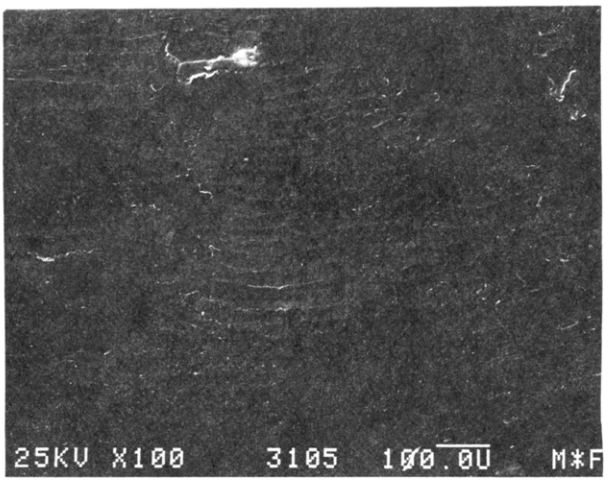

a

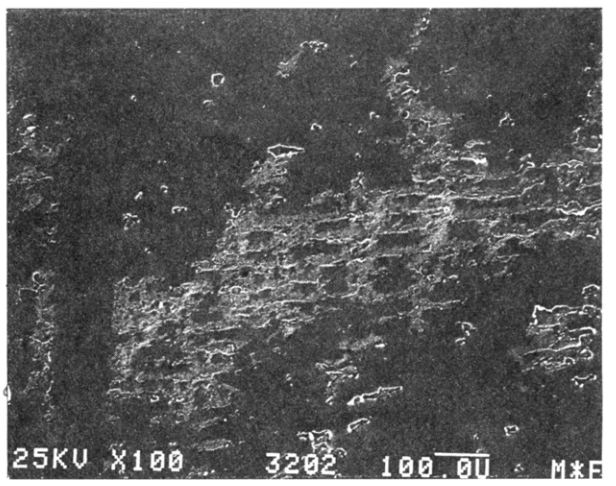

b

Figure 15. SEM micrographs of PMMA fracture surfaces welded to PS: (a) $T_w = 125$ °C; (b) $T_w = 140$ °C. Magnification 100×.

stable crack growth is common in polymers when loaded at very slow rates.[54] The structures of Figure 14 suggest the sticking phase involves the deformation and rupture of the elongated strands while the slipping phase leads to the relatively featureless regions between the deformed ridges.

On the other hand, the corresponding PMMA fracture surfaces are quite different, as shown in Figure 15. In each case, PS residue is evident; the rest of the surface in each photo is rather featureless. The ratio of featureless to ridge material in Figure 15 is about 3:1, which is consistent with the XPS data. However, the resulting fracture energy (ca. 50 J/m^2), computed in terms of virgin strength/adhesive fracture ratios, does not scale with the ratio of adhesive/cohesive areal contributions, probably because the cohesive energy contribution (associated with the ridges) is not the same as that in the virgin material. Comparison of the corresponding PS and PMMA surfaces also indicates that good wetting was achieved.

Examination of the PMMA surfaces at higher magnification suggests that the residues of the polydisperse PS occur when the crack leaves the interface, grows in the PS, and then returns to the interface. It appears the residues correspond to regions where crack growth was "slip"-like, while the "stick" mode resulted in the featureless regions.

Changing the molecular weight of the PS led to different residue morphologies. The features of the 128 000 M_n PS, while showing line-like correlations seen in the polydisperse material, were observed to be more discrete, being in the form of small islands 5–10 μm across. When the PS molecular weight is increased to 575 000, the residue on the PMMA is in the form of randomly distributed islands of PS ranging from 1 to more than 10 μm across.

It is clear from these figures that the weld strength of PS/PMMA interfaces derives from at least two sources: the breakdown of the PS/PMMA interface and the fracture of bulk PS. The first process gives rise to the ridge features seen in Figure 14 and the featureless regions of the PMMA surfaces. The latter one leaves the PS residues seen on the PMMA fracture surfaces. The similarity between the PS fracture surfaces suggests the same crack growth mechanism is dominant in all cases.

SEM Analysis of PSAN/PMMA Fracture Surfaces. In contrast to the PS/PMMA surfaces of the previous section, strong resemblances between the corresponding fracture surfaces were seen in the PSAN/PMMA case. It will be recalled that two of the compositions in this study showed cohesive fractue behavior, indicating fracture did

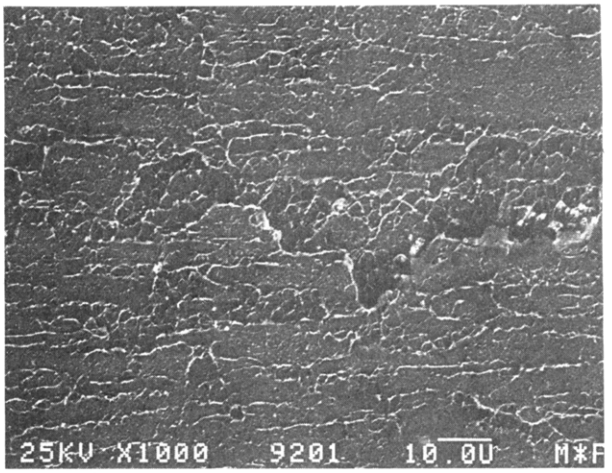

a

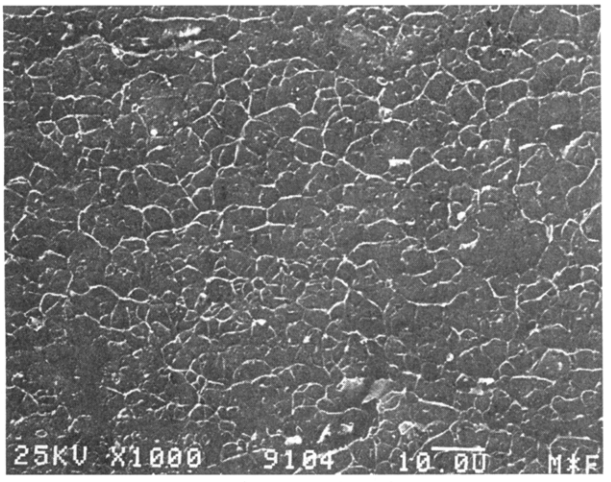

b

Figure 16. SEM micrographs of PSAN/PMMA fracture surfaces: (a) PSAN; (b) PMMA. AN content is 5.7%. T_w = 125 °C. Magnification 1000×.

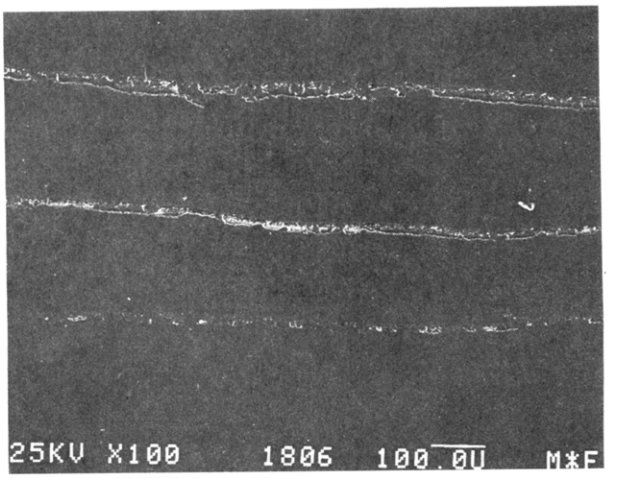

a

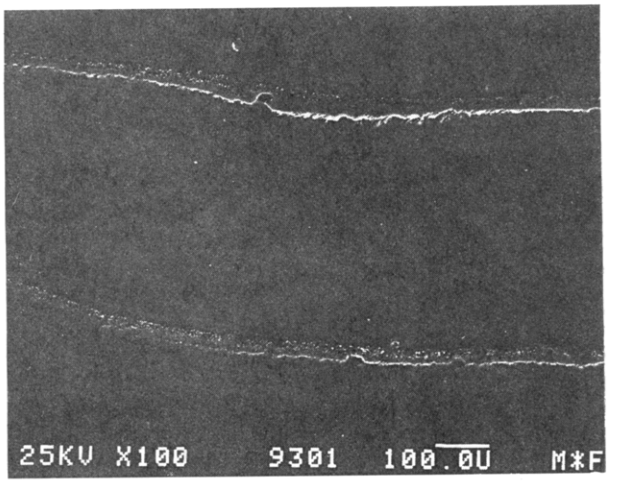

b

Figure 17. SEM micrographs of PSAN/PMMA fracture surfaces: (a) PSAN; (b) PMMA. AN content is 37%. T_w = 125 °C. Magnification 100×.

not occur at the interface. One would therefore expect the fracture surfaces to resemble one another for a given pair of PSAN/PMMA fracture surfaces.

Micrographs of fracture surfaces of the 5.7% PSAN/PMMA interfaces are shown in Figure 16. The similarity between the two surfaces is evident, as one would expect for bulk material fracture. Although it is not obvious in these photos, a periodicity of roughly 10–20 μm is seen when these surfaces are viewed at lower magnification. As discussed previously, this periodicity is indicative of a stick–slip type of crack growth. The fracture surfaces of the compatible PSAN/PMMA pair, with a strength of about 200 J/m^2, were similar in appearance, which is not surprising given the completely cohesive fracture which occurred. Again stick–slip features with a periodicity of roughly 10 μm were observed.

The surfaces of the 37% AN PSAN/PMMA interfaces are markedly different than the others, as shown in Figure 17. Crack growth in this case was quite discontinuous, snapping rapidly for several hundred microns before being arrested. Following a period of slow growth, the crack then snapped again. This behavior gave rise to the banded structure seen in Figure 17. At higher magnification, as shown in Figure 18, extensive deformation is seen in the slow growth bands. This deformation becomes much finer in detail as the slow band grows, and finally the crack snaps again, giving a featureless PMMA surface. That the features seen on the PMMA are in fact PSAN is supported by the fractal-like fibrillar edges around them, indicating they were ripped away from the other surface during fracture. In addition, the corresponding bands on the PSAN have the appearance of troughs, indicating that the crack grew into the PSAN.

The influence of both welding temperature and the interaction parameter χ on the strength of PSAN/PMMA interfaces is largely consistent with the interpenetration scheme. However, microscopic analysis of the resulting fracture surfaces indicates fracture is cohesive in two of the three cases studied. This cohesive nature casts doubt on the interpenetration hypothesis. It will be shown in the next section that the interpenetration picture of interface strength is consistent with cohesive fracture, albeit in an indirect manner.

SEM Analysis of PC/PSAN Fracture Surfaces. Although this pair of polymers is different from the other two systems since welding took place at or below T_g of one

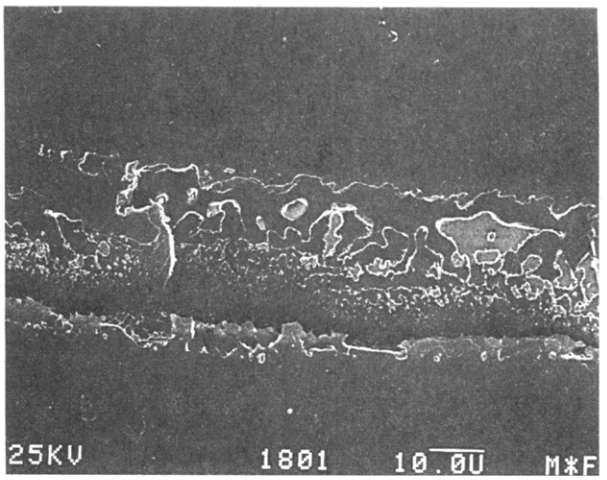

a

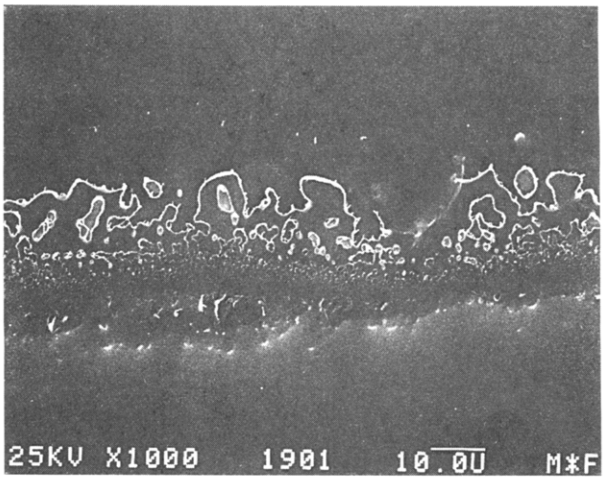

b

Figure 18. SEM micrographs of PSAN/PMMA fracture surfaces: (a) PSAN; (b) PMMA. AN content is 37%. Magnification 1000×.

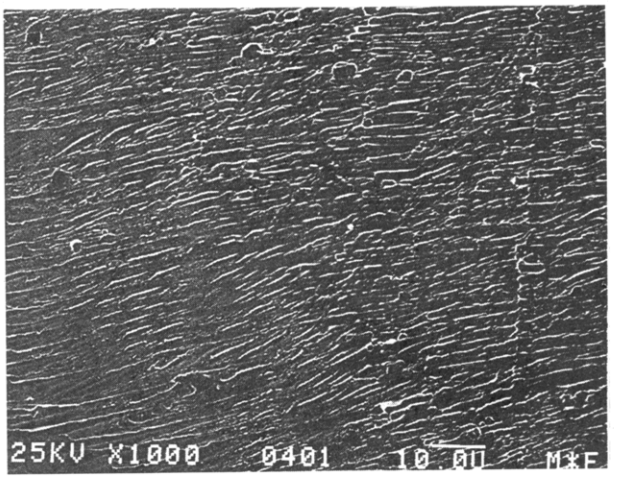

a

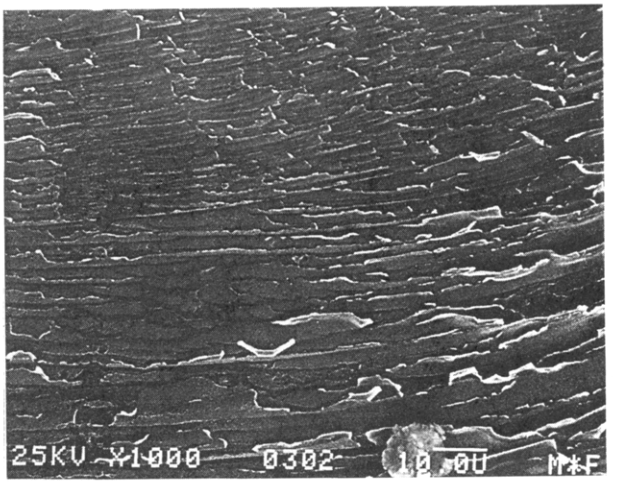

b

Figure 19. SEM micrographs of PC/PSAN fracture surfaces: (a) PSAN; (b) PC. AN content is 23%. Magnification 1000×.

of the components, the PSAN surfaces show characteristics similar to those seen before. Figure 19 illustrates the features seen on the PSAN and PC fracture surfaces. The presence of structures hundreds of microns in length with spacings of 2 or 3 μm is indicative of the familiar stick–slip type of crack growth seen in the previous cases. The similarity of the three PSAN fracture surfaces suggests the same mechanism is in operation at all three interfaces during crack growth.

The PC surfaces welded to the 5.7% AN and 37.0% AN copolymers were relatively featureless, while the PC welded to the 23.0% AN copolymer has large regions of residual copolymer, as shown in Figure 19. In the last section it was shown that this pair gave the largest N/C ratio at each welding temperature, in addition to having the highest weld strength. The source of the N_{1s} signal in Figure 19 is clearly due to residual PSAN. The orientation of the features seen on the PC surface of Figure 19 is quite interesting. The tops of the "ridges" of PSAN point in the direction from which the crack came, not in the direction of crack growth. Clearly then they are not due to the crack simply running off the interface as was seen in the polydisperse PS/PMMA fracture surfaces. It will be shown in the next section that these features are due to the growth of crazes ahead of the crack before fracture occurs.

Discussion

The use of cleavage geometries to characterize isotropic materials is hampered by the fact that cracks run to the specimen surface once they start growing. This behavior is due to the interaction between the bending force acting on the crack surfaces and the tensile force normal to the median plane of the sample. The net result is a maximum tensile stress whose normal makes an angle of roughly 80° with the median plane.[55] It is this plane in which fracture occurs, via craze growth and breakdown in glassy polymers like PS and PMMA, and thus the crack immediately runs away from the middle of an isotropic sample once initiated. Various techniques have been developed to avoid this problem in cleavage specimens.[56]

When a cleavage specimen is wedge loaded, as in the geometry used in this study (Figure 1), an additional compressive force is introduced which acts in the median plane of the sample in the opposite direction of the bending force. Therefore, it shifts the direction of the maximum tensile stress, according to its magnitude; the plane of

fracture is also changed. The fracture of the incompatible polymer interfaces in this study is a result of the interplay between tension, compression and bending, and mode mixing due to differences in modulus E, Poisson's ratio υ, and craze stress σ_c.

The complex stress field and mode mixing at a bimaterial interface with different moduli and Poisson's ratios has been the subject of many studies and has been reviewed by Suo and Hutchinson.[57] Even though a fracture specimen may be loaded in a symmetric manner, differences in moduli in particular result in additional stresses, e.g., shear stress in the plane of the interface, which do not exist in the symmetric interface. These stresses, coupled with the difference in craze formation of the two sides, cause the deformation zone to become asymmetric and allow the crack to propagate in one side or the other. The solution to the problem of coupling the asymmetric deformation zone evolution with the mode-mixing stress field due to E and υ asymmetry, to predict the fracture energy and locus of failure, does not exist.

Good[58] also examined fracture between dissimilar materials (1 and 2) using the Griffith–Irwin crack theory. He examined differences in the elastic moduli $\Delta E = E_1 - E_2$ and bulk fracture energy $\Delta G = G_1 - G_2$. He was able to categorize the type of fracture (adhesive vs cohesive) by the signs of ΔE and ΔG and the strength of the interface. He makes the following points: True interfacial fracture (adhesive) was predicted to occur only when the interfacial strength was low and ΔG and ΔE had opposite signs. If ΔG and ΔE were of the same sign, even interface forces weaker than bulk cohesive ones were found to be sufficient to cause a high probability of cohesive failure. If the interfacial forces were moderately strong, cohesive failure occurred regardless of the signs or relative magnitudes of ΔE and ΔG. The exact locus of failure in this case was determined by ΔE and ΔG.

Brown et al.,[42,43] Creton et al.,[44,61] and Cho et al.[62] examined several asymmetric polymer interfaces where the sample thicknesses ($h_2 - h_1$) were varied. They found, for example, in wedge cleavage fracture of PS/PMMA interfaces that the locus of failure could occur on either side, depending on the thickness of the beams, such that cohesive fracture occurred on the thinner (peeling) side. Furthermore, it was possible to obtain a very low fracture energy (ca. 2–5 J/m^2) by peeling PMMA (with the higher craze stress) from a thick PS substrate. Thus, the magnitude of the measured fracture energy depends on the details of the asymmetry such that the largest fracture energy corresponds to the greatest amount of craze formation during fracture. When craze formation is minimized, fracture can still occur by chain scission and some chain pullout which results in a very low fracture energy.

In our studies, the importance of the dissimilar properties is illustrated by the presence of crazes ahead of the crack, which form in the subcritical stage. Figure 20 illustrates this phenomenon for two systems, the 23% AN PSAN/PC and the 5.7% AN PSAN/PMMA. In both cases, the crazes initiate and grow in the PSAN phase and attain a length of roughly 20 μm by the time fracture occurs. The crazes do not initiate at the interface and grow out into the bulk but rather initiate in a plane roughly 45° to the crack growth direction. Their subsequent curvilinear growth reflects the evolution of the stress field as loading continues.

The tendency of the crazes to become more parallel to the interface indicates the increasing magnitude of the bending force as loading continues and the beams of the sample are spread further apart. The net effect is that the maximum tensile stress axis becomes more perpendicular to the interface plane. Since the interface is weaker than either bulk, it begins to break down and crack growth is initiated if the stress is high enough. Stopping the wedge motion at this point allows the system to dissipate energy via crack growth. If the tensile stress is not great enough to initiate crack growth, further loading increases the bending stress still more. Finally, a stage is reached wherein the stress distribution is similar to that of an isotropic sample, and the crack runs away from the interface, once initiated. This type of failure did indeed occur occasionally with the PSAN/PMMA interfaces which exhibited the highest strengths, with the subsequent loss of the sample.

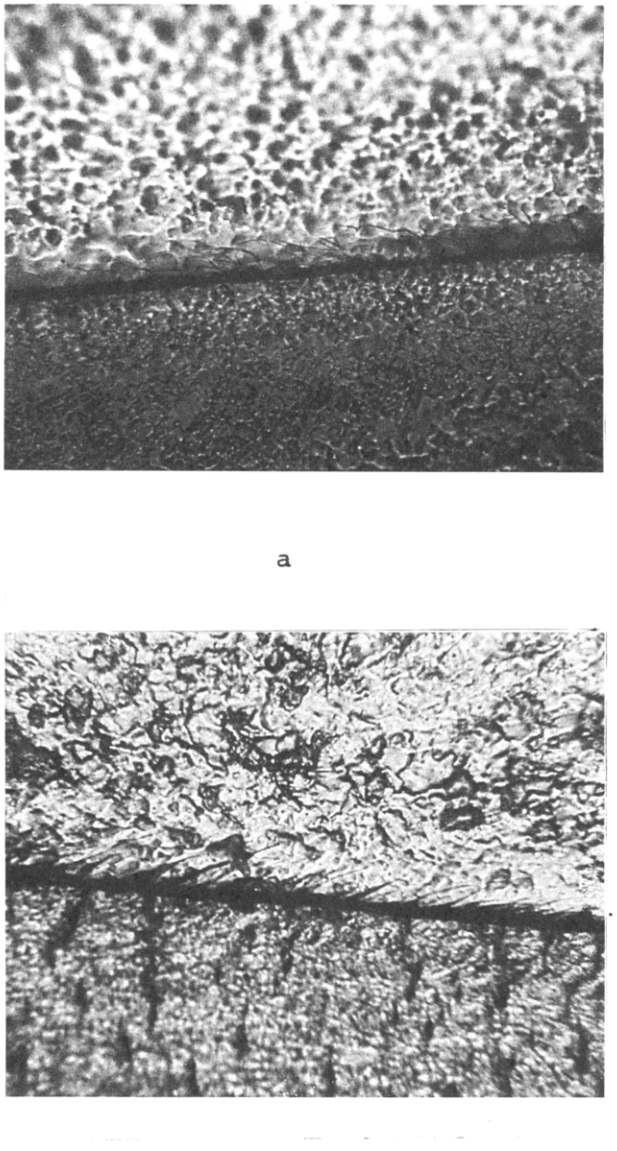

Figure 20. Crazes ahead of crack at incompatible polymer interfaces: (a) PSAN/PMMA (5.7% AN); (b) PC/PSAN (23% AN). In a, the crack grows from left to right; in b, it grows from right to left.

The presence of crazes in front of the crack tip provides an explanation for the features seen on the PC fracture surfaces welded to the 23% AN PSAN (Figure 19). Once crack growth started, the crazes ahead of the crack provided paths for it to leave the interface. As the crack jumped between the crazes, it tore through the noncrazed regions between them before returning to the interface, leaving

Table IV. Entanglement Densities (entanglements/cm³)

polymer	M_e	υ_e (10^{-19})
PS	19 100[a]	3.3
PSAN (5.7% AN)	17 100[d]	3.7
PSAN (23% AN)	11 000[b]	5.9
PSAN (37% AN)	6 100[d]	10.6
PMMA	8 800[b]	8.2
PC	2 500[c]	29.0

[a] Ferry.[64] [b] Wu.[50] [c] Kramer.[59] [d] Estimated from Wu.[50]

behind the ridges observed. No direct evidence of off-axis crazes was seen in the other interfaces studied.

The asymmetry of the deformation zone at the crack tip can be deduced from the relative tendency of each material to form crazes. Kramer and co-workers have shown that the entanglement density determines whether an amorphous polymer will craze or form shear yield deformation zones.[59,60] PS, with a relatively low entanglement density, readily crazes whereas PC, with a much higher one, does not. Table IV lists the entanglement densities of each of the materials used in this work. It is significant to note that, in all cases, a residue of the polymer with the lower entanglement density is found on the fracture surface of its welding partner, regardless of differences in moduli and T_gs. The only exception to this trend is the 37% AN PSAN/PMMA pair, but some uncertainty exists in the correct value of M_e for this copolymer. Also of significance is the fact that, where crazing was observed, it always happened in the lower entanglement density side (Figure 20). On the basis of the structure of entanglements,[1,65] we expect the craze stress to depend on $M_e^{-1/2}$, as noted by Wu.[50]

The effect of entanglement density on crazing is one possible explanation for the discrepancy in the normalized N/C ratios of PC fracture surfaces and ultimate weld strength. In the previous section, it was shown that the PC surface welded to the 5.7% AN PSAN had more PSAN residue than the PC surface welded to the 37% AN PSAN, even though its interfacial strength was lower. Since the former copolymer is expected to craze more readily due to a lower entanglement density, craze growth before fracture may produce more pathways for cohesive fracture compared with the latter copolymer. The net result is then a greater amount of the lower AN content copolymer on the PC fracture surface. Three-point bend tests verified this relative crazing behavior.

Robertson[63] observed crazes at PS/PMMA interfaces when the two materials were solvent bonded. Although unable to verify it, he concluded the crazes were primarily in the PMMA. From this conclusion, he surmised "good molecular contact" is all that is needed to achieve an interface whose resistance to crazing is the same as the bulk materials. It is clear from the results above, however, that, for thermally welded PS/PMMA interfaces, the PS undergoes more deformation during the fracture process. Therefore, one can conclude that while good molecular contact may be sufficient to induce plastic deformation in the adjacent bulk, it is not enough to raise the interface strength to that of the bulk.

Summary

The development of mechanical strength at incompatible polymer interfaces was investigated. Three pairs of polymers were studied: PS/PMMA, PSAN/PMMA, and PC/PSAN in which the AN content was varied. All three pairs consist of glassy amorphous polymers which may be thermally welded above T_g and tested in the glassy state at room temperature. The following points are made in summary:

1. A molecular description of incompatible polymer interfaces was given using the mean-field theories of Helfand et al. These theories predict that such interfaces are not sharp, as in small-molecule systems, but consist of a diffuse region of finite equilibrium thickness d_∞, where $d_\infty \sim 1/\sqrt{\chi}$. When coupled with a microscopic welding model where $G_{1c} \sim d_\infty$,[2] this molecular description of the interface predicts that the fracture energy behaves as $G_{1c} \sim 1/\chi$. In addition, since χ is a quadratic function of composition for copolymer/homopolymer pairs, changes in composition and temperature should be reflected by changes in G_{1c}.

2. The relationship between G_{1c} and χ was confirmed in all three systems investigated. The weld strength increased with welding temperature, except for the PS/PMMA pair where the χ parameter was not very temperature dependent. The strength of PSAN/PMMA interfaces increased as χ decreased with the AN content. The copolymer with 23% AN was compatible with PMMA and here $G_{1c} \sim t^{1/2}$. For PC/PSAN interfaces, a maximum in G_{1c} was seen at 23% AN, which corresponded to the minimum in χ calculated using solubility parameters.

3. X-ray photoelectron spectroscopy analysis showed that fracture was in all cases cohesive to some extent and was completely cohesive for two of the PSAN/PMMA interfaces. The cohesive failure always occurred on only one side of the interface. In addition, corresponding fracture surfaces were found to be dissimilar in appearance when examined by electron and optical microscopy. The polymers in which cohesive failure occurred showed extensive deformation and evidence of stick–slip crack growth. The surfaces to which they were welded showed few features except for residues from the other polymer. Only the fracture surfaces of the completely cohesive failures were similar in appearance.

4. In all cases, a correlation was established between the polymer in which cohesive failure took place and the entanglement density. The polymer with the lower entanglement density always experienced cohesive failure. In addition, these polymers exhibited large deformations at the interface, as well as evidence of stick–slip crack growth. These observations are in agreement with those of Kramer and co-workers, who noted that polymers with low entanglement densities craze, while those with higher entanglement densities form shear yielded deformation zones.

5. The magnitude of the fracture energy and the locus of failure of asymmetric interfaces involves factors arising from both mode mixing (incurred with differences in υ and E) and the evolution of an asymmetric deformation zone (due to differences in craze initiation stress, entanglement density, craze thickening rates, etc.). If the moduli are the same, then the formation of an asymmetric deformation zone due to differences in craze stress should control the locus of fracture near the interface, depending on the interface strength. If the moduli are different, the locus of failure will be a competition between differences in craze initiation stresses and the stress field driving the crack off the interface plane into the softer side. If the soft side has a lower craze stress, then cohesive failure will tend to occur on this side. However, if the soft side has a higher craze stress, then the locus of failure will be closer to the interface plane.

Acknowledgment. The authors express their gratitude to the Army Research Office, Grant DAAL03-86-K-0034, and to Dow Chemical Co. for support of this work and to C. B. Arends and S. Martin of Dow for their assistance and discussions. R.P.W. received partial support from

the Air Force Office of Scientific Research, Grant AFOSR-90-0242. We are grateful to Dr. C. Kozlowski and Judy Baker of the University of Illinois Materials Research Laboratory for assistance in the XPS measurements and analysis via a grant from the National Science Foundation, DMR-89-20538. The Center for Microanalysis of Materials is supported by the U.S. Department of Energy Contract DE-AC02-76ER-01198. R.P.W. particularly acknowledges helpful discussions of this work with Drs. Hugh Brown and C. Creton and Professor Ed. Kramer.

References and Notes

(1) Wool, R. P. *Structure and Strength of Polymer Interfaces*; Hanser Press: New York, in press.
(2) Prager, S.; Tirrell, M. *J. Chem. Phys.* **1981**, *75*, 5194.
(3) Adolf, D.; Tirrell, M.; Prager, S. *J. Polym. Sci., Polym. Phys. Ed.* **1985**, *23*, 413.
(4) Kim, Y.-H.; Wool, R. P. *Macromolecules* **1983**, *16*, 1115.
(5) de Gennes, P.-G. *C. R. Seances Acad. Sci., Ser. B* **1980**, *291*, 219.
(6) Jud, K.; Kausch, H. H. *Polym. Bull.* **1979**, *1*, 697.
(7) Jud, K.; Kausch, H. H.; Williams, J. G. *J. Mater. Sci.* **1981**, *16*, 204.
(8) Wool, R. P.; O'Connor, K. M. *J. Appl. Phys.* **1981**, *52*, 5953; *J. Polym. Sci., Polym. Lett. Ed.* **1982**, *20*, 7.
(9) Wool, R. P.; Yuan, B.-L.; McGarel, O. J. *Polym. Eng. Sci.* **1989**, *29*, 1340.
(10) Roland, C. M.; Bohm, G. G. *J. Appl. Phys.* **1984**, *29*, 3803.
(11) Skewis, J. D. *Rubber Chem. Technol.* **1966**, *39*, 217.
(12) Forbes, W. G.; McLeod, L. A. *Trans. IRI* **1958**, *30*, 154.
(13) de Gennes, P.-G. *C. R. Hebd. Seances Acad. Sci.* **1981**, *292*, 1505.
(14) Brochard, F.; Louffroy, J.; Levinson, P. *Macromolecules* **1983**, *16*, 1683.
(15) Foley, G.; Cohen, C. *J. Polym. Sci., Polym. Phys. Ed.* **1987**, *25*, 2027.
(16) Kramer, E. J.; Green, P.; Palmstrom, C. J. *Polymer* **1983**, *25*, 473.
(17) Kausch, H. H.; Petrovska, D.; Landel, R. F. *Polym. Sci. Eng.*, in press.
(18) Fowler, M. E.; Barlow, J. W.; Paul, D. R., results to be published.
(19) Helfand, E.; Tagami, Y. *J. Chem. Phys.* **1972**, *56*, 3592.
(20) Helfand, E.; Sapse, A. M. *J. Chem. Phys.* **1975**, *62*, 1327.
(21) Kammer, H. W. *Z. Phys. Chem. (Leipzig)* **1977**, *258*, 1149.
(22) Binder, K.; Frisch, H. L. *Macromolecules* **1984**, *17*, 2928.
(23) McLaren, A. D. *J. Polym. Sci.* **1948**, *3*, 652.
(24) Voyutskii, S. S.; Shapalova, A. I.; Pisarenko, A. P. *Colloid J. (U.S.S.R.)* **1957**, *19*, 279.
(25) Voyutskii, S. S. *Rubber Chem. Technol.* **1960**, *33*, 748.
(26) Voyutskii, S. S.; Vakula, V. L. *J. Appl. Polym. Sci.* **1963**, *7*, 475.
(27) Inegar, Y.; Erickson, D. E. *J. Appl. Polym. Sci.* **1967**, *11*, 2311.
(28) Voyutskii, S. S. *Autohesion and Adhesion of High Polymers*; John Wiley and Sons: New York, 1963.
(29) Voyutskii, S. S.; Yagnyatinskaya, S. M.; Kaplunova, L.; Garetovskaya, N. L. *Rubber Age* **1973**, *37*.
(30) Wu, S. *Polymer Interface and Adhesion*; Dekker: New York, 1982.
(31) O'Connor, K. M. Ph.D. Thesis, University of Illinois, 1984.
(32) Robertson, R. E. Toughness and Brittleness of Plastics. *Advances in Chemistry Series 154*; American Chemical Society: Washington, DC, 1976.
(33) Willett, J. L. Ph.D. Thesis, University of Illinois, 1988.
(34) Foster, K.; Wool, R. P. *Macromolecules* **1991**, *24*, 1397.
(35) Whitlow, S.; Wool, R. P. *Macromolecules* **1989**, *22*, 2648; **1991**, *24*, 5926.
(36) Wool, R. P. *Rubber Chem. Technol.* **1984**, *57*, 307.
(37) Russell, T. P.; Menelle, A.; Hamilton, W. A.; Smith, G. S.; Satija, S. K.; Majkrzak, C. F. *Macromolecules* **1991**, *24*, 5721.
(38) Adamson, A. W. *Physical Chemistry of Surfaces*; John Wiley and Sons: New York, 1982.
(39) Fowkes, F. M.; Tischler, D. O.; Wolfe, J. A.; Lannigan, L. A.; Ademu-John, C. M.; Halliwell, M. J. *J. Polym. Sci., Polym. Chem. Ed.* **1984**, *22*, 547.
(40) Drago, R. S.; Vogel, G. C.; Needham, T. E. *J. Am. Chem. Soc.* **1971**, *93*, 6014.
(41) Brochard-Wyart, F.; de Gennes, P.-G.; Troian, S. *C. R. Seances Acad. Sci. Ser. II* **1990**, *310*, 1169.
(42) Brown, H. R. *Macromolecules* **1991**, *24*, 2752.
(43) Brown, H. R. *J. Mater. Sci.* **1990**, *25*, 2791.
(44) Creton, C.; Kramer, E. J.; Hui, C.-Y.; Brown, H. R. *Macromolecules* **1992**, *25*, 3075.
(45) Kressler, J.; Kammer, H. W.; Klosterman, K. *Polym. Bull.* **1986**, *15*, 113.
(46) Balazs, A. C.; Sanchez, I. C.; Epstein, I. R.; Karasz, F. E.; MacKnight, W. J. *Macromolecules* **1985**, *18*, 2188.
(47) Balazs, A. C.; Karasz, F. E.; MacKnight, W. J.; Ueda, H.; Sanchez, I. C. *Macromolecules* **1985**, *18*, 2784.
(48) Curro, J. G.; Schweizer, K. S. *Macromolecules* **1991**, *24*, 6737.
(49) Fowler, M. E.; Barlow, J. W.; Paul, D. R. *Polymer* **1987**, *28*, 1177.
(50) Wu, S. *Polymer* **1987**, *28*, 1144.
(51) Keitz, J. D.; Barlow, J. W.; Paul, D. R. *J. Appl. Polym. Sci.* **1984**, *29*, 3131.
(52) Mendelson, R. A. *J. Polym. Sci., Polym. Phys. Ed.* **1985**, *23*, 1975.
(53) Brundle, C. R. *J. Vac. Sci. Technol.* **1974**, *11*, 212.
(54) Kinloch, A. J. *Met. Sci.* **1980**, *14*, 305.
(55) Guernsey, R.; Gilman, J. *Exp. Mech.* **1961**, *1*, 50.
(56) Berry, J. P. *J. Appl. Phys.* **1963**, *34*, 62.
(57) Suo, Z.; Hutchinson, J. W. *Int. J. Fract.* **1990**, *43*, 10.
(58) Good, R. J. *J. Adhes.* **1972**, *4*, 133.
(59) Kramer, E. J. *Polym. Eng. Sci.* **1984**, *24*, 761.
(60) Donald, A. M.; Kramer, E. J. *J. Mater. Sci.* **1981**, *16*, 1967; **1981**, *16*, 2977; **1982**, *17*, 1871.
(61) Creton, C.; Kramer, E. J. *Macromolecules* **1991**, *24*, 1846.
(62) Cho, K.; Brown, H. R.; Miller, D. C. *J. Polym. Sci., Polym. Phys.* **1990**, *28*, 1699.
(63) Robertson, R. E. *J. Adhes.* **1972**, *4*, 1.
(64) Ferry, J. D. *Viscoelastic Properties of Polymers*, 2nd ed.; John Wiley and Sons: New York, 1986.
(65) Wool, R. P. *Macromolecules* **1993**, *26*, 1564.